frontiers | Frontiers in Materials

ORIGINAL RESEARCH
published: 06 July 2022
doi: 10.3389/fmats.2022.931682

Lactobionic Acid-Navigated Gold Nanorods With Light-Triggered "on-Demand" Drug Release for Synergistic Photothermal-Chemotherapy

Zhang Zhang and Chunyang Sun *

Department of Radiology and Tianjin Key Laboratory of Functional Imaging, Tianjin Medical University General Hospital, Tianjin, China

The rational design of the nanocarriers with active tumor targeting and specific chemotherapy for heat shock protein 90 (Hsp90) inhibition is attractive for combined chemo-photothermal therapy (PTT). Herein, a smart gold nanorod (GNR)-cored micelle (T-GNR_{AAG}) was developed to encapsulate 17-allylamino-17-demethoxygeldanamycin (17-AAG, Hsp90 inhibitor) through a facile preparation approach. The characteristics of T-GNR_{AAG} were evaluated both *in vitro* and *in vivo*. The designed nanoplatform possessed sufficient 17-AAG loading content and lactobionic acid-mediated active targeting for hepatoma cells. More importantly, the 808 nm laser irradiation not only initiated PTT for cell killing but also remotely triggered 17-AAG liberation within cancer cells *via* inducing the phase transition of poly(ε-caprolactone). All these features forcefully supported the effectiveness of T-GNR_{AAG} in tumor growth inhibition. This work represents a proof-of-concept combinatorial chemo-PTT treatment.

Keywords: lactobionic acid targeting ligand, gold nanorod, chemotherapy and photothermal therapy, on-demand drug release, Hsp90 inhibitor

OPEN ACCESS

Edited by:
Huaqiong Li,
University of Chinese Academy of Sciences, China

Reviewed by:
Junjie Li,
Innovation Centre of NanoMedicine (iCONM), Japan
Chang-Ming Dong,
Shanghai Jiao Tong University, China

***Correspondence:**
Chunyang Sun
chysun412@163.com

Specialty section:
This article was submitted to Biomaterials, a section of the journal Frontiers in Materials

Received: *29 April 2022*
Accepted: *01 June 2022*
Published: *06 July 2022*

Citation:
Zhang Z and Sun C (2022) Lactobionic Acid-Navigated Gold Nanorods With Light-Triggered "on-Demand" Drug Release for Synergistic Photothermal-Chemotherapy. Front. Mater. 9:931682. doi: 10.3389/fmats.2022.931682

INTRODUCTION

Photothermal therapy (PTT), which absorbs optical energy and then converts it to the thermal effect, has attracted great attention for cancer therapy because of its highly noninvasive nature, controllability, and repeatability (Abadeer and Murphy, 2016; Doughty et al., 2019; Xi et al., 2020; Zhang et al., 2021). Upon laser irradiation with deep penetration in the body, the tumoral cells would be specifically ablated by the raised temperature in tumor sites (Wang et al., 2019; Dong et al., 2020; Sun et al., 2021). Up to now, various nanoparticles with photothermal conversion have been proposed to serve as anticancer agents, such as gold nanorods (GNRs), gold nanoshells, carbon nanotubes, conjugated polymers, and small molecules (Jang et al., 2011; Chen et al., 2016; He et al., 2020a; He et al., 2020b; Li and Pu, 2020"). Except for the photothermal effect itself, phototherapeutic agents have been widely utilized in combination with chemotherapy for more advanced antitumor efficiency through distinct molecular mechanisms (Yang J-.C. et al., 2017; Xie et al., 2020; Yang et al., 2021). Even more interesting is that the photothermal effect could not only directly kill the cancer cells but also boost the chemotherapeutic agent liberation specifically in the irradiated area, thereby achieving locoregional and precise chemo-PTT. For instance, Liu et al. designed GNR-cored micelles (AuNR-M-DOX) to realize photo-triggered drug release for overcoming the multidrug resistance in

MCF-7/ADR cells (Zhong et al., 2013). Tan et al. intercalated doxorubicin into a DNA immobilized on GNRs and particularly liberated it inside the cancer cells *via* photocontrollable thermal effect and DNA unwinding (Yi et al., 2017).

Despite great efforts, PTT has been found to be limited by overexpression of heat shock protein 90 (Hsp90) (Gao et al., 2019; Sun et al., 2019; Chen et al., 2020). During the PTT process, Hsp90 is usually upregulated in tumoral cells and is responsible for protecting the client proteins from stress-induced cellular damage (Whitesell and Lindquist, 2005; Lamb et al., 2006; Shan et al., 2021). The overexpression of Hsp90 will result in the heat resistance acquired by cancer cells and thus remarkably weaken PTT efficacy (Yang Y. et al., 2017; Li L. et al., 2020). Therefore, inhibiting the expression or function of Hsp90 is crucial for improving the efficiency of PTT (Lin et al., 2016; Long et al., 2018). Fortunately, 17-allylamino-17-demethoxygeldanamycin (17-AAG), one of the geldanamycin derivatives, has been widely studied as the Hsp90 inhibitor (Kamal et al., 2003; Saxena, et al., 2012; Liu Y. et al., 2019). 17-AAG specifically binds to the amino-terminal ATP binding pocket of Hsp90 in cancer cells and inhibits the stabilization between Hsp90 and its client proteins (Ferrario and Gomer, 2010; Hasenstein et al., 2012). Since most Hsp90 client proteins (e.g., EGFR and AKT) contribute to tumor growth, 17-AAG is obviously toxic to cancer cells (Modi et al., 2011; Rochani et al., 2016). However, its application as a chemotherapeutic agent remains a significant challenge owing to the rapid blood clearance and lack of targeting to tumor tissue *in vivo* (Waza et al., 2005).

To this end, we report a GNR platform capable of lactobionic acid (LA)-mediated targeting for hepatoma cells and light-controlled 17-AAG release for improving chemo-PTT efficiency (**Figure 1**). Because of its robust affinity to asialoglycoprotein receptor, which is overexpressed on hepatoma cells, LA has been considered as a promising ligand for targeted drug delivery to hepatocellular carcinoma (Liu H. et al., 2014; Zhang et al., 2019; Huang et al., 2020). With the help of LA moiety, the designed nanoparticles (T-GNR_{AAG}) could achieve selective accumulation in HepG2 tumors after intravenous injection. Following internalization into tumoral cells *via* interaction between LA and asialoglycoprotein receptor, 808 nm laser irradiation would produce a mild PTT against HepG2 cells, and the raised temperature on the GNR surface would trigger the phase transition of the PCL component to liberate hydrophobic 17-AAG. Subsequently, 17-AAG could not only act as an Hsp90 inhibitor to induce cell cycle arrest and apoptosis but also sensitize cancer cells to PTT through regulating the pro-survival and angiogenic signaling pathways, hence realizing the synergistic chemo-PTT in the specific cells that underwent PTT (Georgakis et al., 2006; Li and Katoka, 2021; Zhu et al., 2021). The cascade-amplified chemo-PTT of T-GNR_{AAG} and its benefits under 808 nm laser irradiation were evaluated on HepG2 tumor-bearing mice.

MATERIALS AND METHODS

Materials

Sodium borohydride, cetyltrimethyl ammonium bromide (CTAB), ascorbic acid, silver nitrate, and tetrachloroauric acid were purchased from Sinopharm Chemical Reagent Co., Ltd. CTAB-stabilized GNRs were synthesized according to reported methods (Li et al., 2013). LA functional poly(ethylene glycol)-poly(ε-caprolactone)-SH (LA-PEG-PCL-SH) and poly(ethylene glycol)-poly(ε-caprolactone)-SH (PEG-PCL-SH) were obtained from Xi'an Ruixi Biological Technology Co., Ltd. Cell Counting Kit-8 (CCK-8) was purchased from Abcam Co., Ltd. Dulbecco's modified Eagle's medium and fetal bovine serum were purchased from Life Technologies Corporation (Gibco, United States). All other reagents were purchased from Shanghai Aladdin Bio-Chem Technology Co., LTD., and used as received.

Preparation of 17-AAG-Loaded T-GNR

Typically, the CTAB-stabilized GNRs were washed and purified by centrifugation (14,500 rpm, 10 min) twice to remove excess CTAB. Then, the organic DMSO containing the LA-PEG-PCL-SH and PEG-PCL-SH copolymer (1:5, molar ratio) was slowly added into CTAB-stabilized GNR aqueous dispersion under vigorous stirring. After reacting for 6 h at room temperature, the T-GNR was purified through centrifugation and washing with ddH_2O twice. Finally, the DMSO containing 17-AAG was mixed with T-GNR aqueous (phosphate buffer, 10 mM, pH 7.4) dispersion under mile stirring. After reaction for overnight, free 17-AAG was removed by dialysis against PB at 4°C in the dark (MWCO: 3,500 Da), and the obtained nanoparticles were denoted by T-GNR_{AAG}. Meanwhile, the nontargeted GNR_{AAG} was prepared following a similar method just only using PEG-PCL-SH for surface decoration.

Cellular Uptake of Targeted Nanocarriers

HepG2 cells in 12-well plates (50,000 cells per well) were incubated with GNR_{AAG} or T-GNR_{AAG} for 4 h. After the incubation, the cells were washed with PBS twice and treated with 0.1% Triton X-100. The internalized 17-AAG and GNRs in cell lysis were detected by UV-vis spectrophotometry and inductively coupled plasma-mass spectrometry (ICP-MS), respectively. For the confocal laser scanning microscope (CLSM) observation, ICG was encapsulated in GNRs instead of 17-AAG because 17-AAG was difficult in a fluorescence imaging application. HepG2 cells were seeded and incubated with GNR_{ICG} or T-GNR_{ICG} for 4 h. Following 4 h of incubation, the cells were washed and fixed with 4% paraformaldehyde and then stained with Alexa Fluor® 488 phalloidin and DAPI sequentially following the standard protocol. The cells were then visualized and imaged on a Zeiss LSM 810 microscope.

Cell Killing of T-GNR_{AAG} Under Laser Irradiation *In Vitro*

To determine the biocompatibility of GNRs, HepG2 cells were seeded in a 96-well plate (10,000 cells per well) and incubated with GNR or T-GNR for 72 h. The cell viabilities were analyzed using a standard CCK-8 assay. To study the combined chemo-PTT efficiency, HepG2 cells were seeded in a 96-well plate (5,000 cells per well). Then, the cells were incubated with free 17-AAG, GNR, T-GNR, GNR_{AAG}, or T-GNR_{AAG} for 24 h. Following the replacement of blank medium without drug or nanoparticles, the

cells were exposed to an 808 nm laser (200 mW/cm^2, 10 min). The cell viabilities were analyzed using a standard CCK-8 assay after further incubation for 48 h.

Pharmacokinetic and Tumor Targeting of T-GNR$_{AAG}$ *In Vivo*

To study the retention of T-GNR$_{AAG}$ *in vivo*, BALB/c mice were randomly divided into three groups (n = 4). The mice received *i.v.* injection of free 17-AAG, GNR$_{AAG}$, or T-GNR$_{AAG}$ (equivalent [17-AAG] = 10 μg/g body weight). At a predetermined time point postinjection (0.17, 0.5, 1, 2, 4, 8, 12, 24, and 48 h), blood samples were collected from the retroorbital plexus. After the centrifugation (3,000 rpm, 10 min), the plasma was collected and 17-AAG concentration was detected using UV-vis spectrophotometry.

To investigate the distribution in different organs of T-GNR$_{AAG}$ *in vivo*, BALB/c nude mice bearing HepG2 tumor xenografts were treated with *i.v.* injection of free 17-AAG, GNR$_{AAG}$ or T-GNR$_{AAG}$ (equivalent [17-AAG] = 10 μg/g body weight). At a predetermined time point postinjection (12, 24, and 48 h), the major organs and tumor tissues were harvested, washed, and weighed, and the gold atom concentration was quantified by ICP-MS.

Antitumor Activity *In Vivo*

HepG2 tumor-bearing BALB/c nude mice were randomly divided into six groups (n = 5). On the day when the tumor volume reached ~100 mm^3, the mice were treated with PBS, free 17-AAG, GNR, T-GNR, or T-GNR$_{AAG}$ ([17-AAG] = 5.0 μg/g body weight) by *i.v.* injections. The tumor lesion was then exposed to an 808 nm laser (0.2 W/cm^2, 10 min). The tumor size and mice body weight were monitored every 3 days. The tumor volume was calculated as 0.5 × length × width^2. The blood sample was collected after the treatment (day 18) for ALT, AST, and BUN detection.

RESULTS AND DISCUSSIONS

Preparation and Characterization of T-GNR$_{AAG}$

To prepare T-GNR with hydrophobic 17-AAG loading, CTAB-stabilized GNRs were first modified and coated with both PEG-PCL-SH and LA-PEG-PCL-SH at a molar ratio of 5:1. The unconjugated copolymers were removed by centrifugation. Then, the hydrophobic 17-AAG was encapsulated into T-GNR hydrophobic–hydrophobic interactions. The drug loading content of 17-AAG was determined using UV-vis spectra as 6.73%, and it could be increased to ~15% by raising the feeding ratio. The transmission electron microscopy observation (**Figure 2A**) revealed that T-GNR$_{AAG}$ was well dispersed with a uniform dimension of approximately 30 nm in length and 6 nm in width. In addition, the nontargeted GNR$_{AAG}$ was prepared following a similar route using only PEG-PCL-SH for surface modification. Owing to the protection and stabilization by the PEG component, both GNR$_{AAG}$ and T-GNR$_{AAG}$ maintained their stability even in PBS (pH 7.4) for 168 h (**Figure 2B**).

To assess the photothermal activity of T-GNR$_{AAG}$ and GNR$_{AAG}$, the temperature change of the T-GNR$_{AAG}$ and GNR$_{AAG}$ aqueous solution was monitored for 10 min, while the PBS was used as a negative control group. As displayed in **Figure 2B**, both the T-GNR$_{AAG}$ and GNR$_{AAG}$ groups exhibited laser power-dependent temperature elevation. The solution temperature was increased from 25.2°C to 55.1°C under 808 nm laser irradiation (1.0 W/cm^2, 10 min) when the [T-GNR$_{AAG}$] was 30 μg/ml. However, there was negligible temperature change for the PBS group, which could be attributed to the lower laser power we used. In addition, the IR thermal images further demonstrated the abovementioned results, and the temperature of the irradiated region of the T-GNR$_{AAG}$ and GNR$_{AAG}$ groups was ca. 30°C. According to the cooling curve (**Supplementary Figure S1**), the photothermal conversion efficiency of GNR$_{AAG}$ and T-GNR$_{AAG}$ calculated using the reported method was 39.7 and 42.7% at 808 nm (Liu S. et al., 2019), respectively, which is comparable to that of reported GNR (Almada et al., 2017).

808 nm Laser-Triggered 17-AAG Release

The hydrophobic 17-AAG was encapsulated and restrained in the amorphous PCL regions of micellar PEG-PCL outside the T-GNR$_{AAG}$. Upon 808 nm laser irradiation, the PTT effect (~60°C) would melt the hydrophobic PCL domain, leading to lower micellar stability and boosted 17-AAG diffusion (Zhong et al., 2013; Liu J. et al., 2014). To verify this assumption, we first measured the melting temperature (T_m) of GNR$_{AAG}$ and T-GNR$_{AAG}$ *via* differential scanning calorimetry. In comparison with bulk PCL homopolymer, whose T_m is ~60°C (He et al., 2004), both GNR$_{AAG}$ and T-GNR$_{AAG}$ showed a slightly decreasing T_m (~55°C, **Supplementary Figure S2**). The 17-AAG release profile was then evaluated by immersing the GNR$_{AAG}$ and T-GNR$_{AAG}$ in the aqueous solution at different temperatures. As illustrated in **Figure 3A**, a robust 17-AAG release behavior was observed when the temperature was above 55°C, which is consistent with the melting temperature (T_m) of GNR-cored micelles. Finally, the quantitative 17-AAG release under 808 nm laser exposure was studied at a 0.2 W/cm^2 power density for 5 min. The pulsed laser irradiation led to 59.29 ± 3.35% and 64.42 ± 3.84% of 17-AAG release from GNR$_{AAG}$ and T-GNR$_{AAG}$ at 4 h, respectively (**Figure 3B**). In contrast, only ~6.09% of total 17-AAG was detected from both nanocarriers without laser treatment. More importantly, the solution temperature of GNR$_{AAG}$ and T-GNR$_{AAG}$ was only increased by ~5.7°C and was significantly lower than the T_m of PCL homopolymer. Collectively, the NIR irradiation is not enough to obviously warm the aqueous solution but could initiate a sufficient local photothermal effect (>55°C) on GNR surface and subsequently melt the coating PCL domain to boost 17-AAG release.

Cellular Internalization of HepG2 Cells

In order to measure the targeted delivery of LA-modified T-GNR$_{AAG}$, HepG2 cell line (human hepatocarcinoma cell

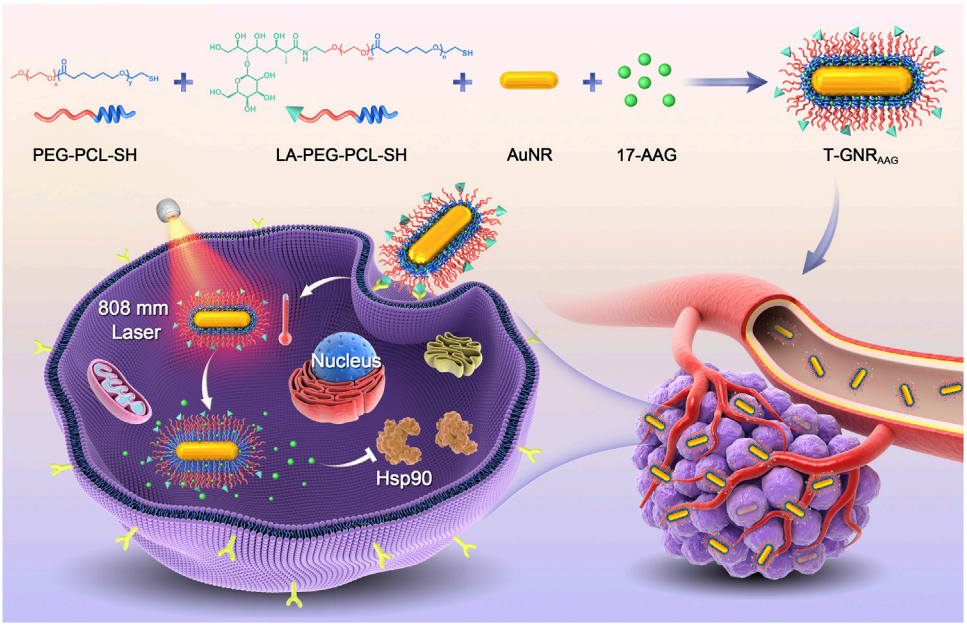

FIGURE 1 | Scheme of LA-targeted drug delivery and 808 nm laser-triggered AAG release for combined chemo-PTT.

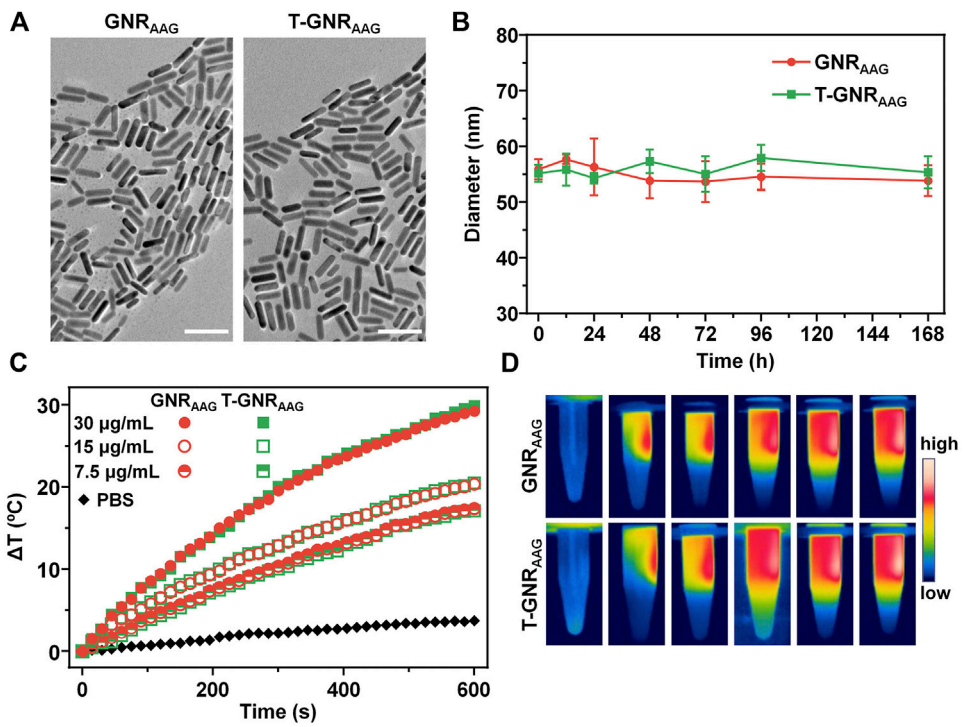

FIGURE 2 | (A) Transmission electron microscope of GNR$_{AAG}$ and T-GNR$_{AAG}$. The scale bar is 50 μm. **(B)** Change of hydrodynamic size in PBS solution (10 mM, pH 7.4). **(C)** Temperature change curves of GNR$_{AAG}$ and T-GNR$_{AAG}$ under 808 nm laser irradiation (1.0 W/cm^2) at different concentrations. **(D)** IR thermal images of GNR$_{AAG}$ and T-GNR$_{AAG}$ (30 μg/ml) under laser irradiation (808 nm, 1.0 W/cm^2).

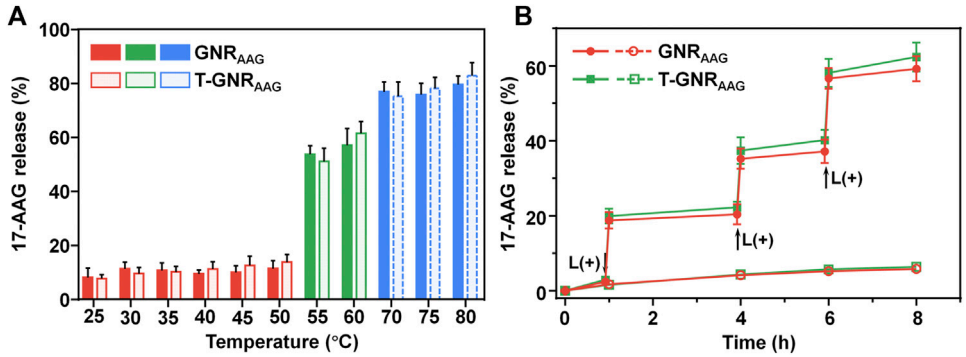

FIGURE 3 | (A) The 17-AAG release pattern from GNR$_{AAG}$ and T-GNR$_{AAG}$ in aqueous solutions at different temperatures. **(B)** 808 nm laser-stimulated pulsed 17-AAG release from GNR$_{AAG}$ and T-GNR$_{AAG}$. The samples were irradiated with an 808 nm laser at specific time points indicated by the arrows.

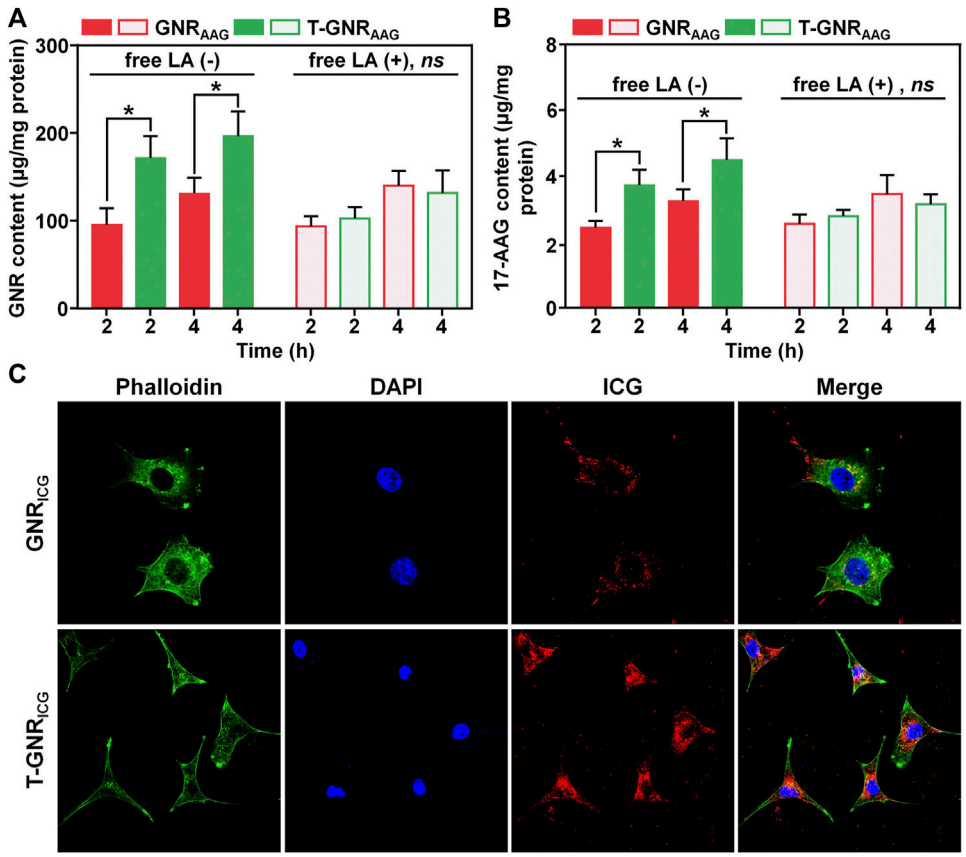

FIGURE 4 | Quantitative cellular uptake of GNR$_{AAG}$ and T-GNR$_{AAG}$ on HepG2 cells detected by ICP-MS **(A)** and UV-vis spectrophotometry **(B)**. (C) CLSM observation of internalization of GNR$_{ICG}$ and T-GNR$_{ICG}$ on HepG2 cells. DAPI (blue) and Alexa Fluor 488 phalloidin (green) were used to stain cell nuclei and F-actin, respectively.

line) was chosen to study the active targeting for internalization. The HepG2 cells were incubated with different formulations for 4 h, and the intracellular gold atom and 17-AAG content were determined by ICP-MS and UV-vis spectrophotometry, respectively. As displayed in **Figure 4A**, the gold atom concentration in lysis of HepG2 cells incubated with T-GNR$_{AAG}$ for 4 h (196.64 ± 27.99 μg/mg protein) was significantly higher than that of GNR$_{AAG}$ (131.04 ± 17.82 μg/mg protein), indicating that LA ligands substantially recognized the receptor on the cellular membrane and improved the cellular internalization. Meanwhile, the UV-vis spectrophotometry results in **Figure 4B** further demonstrated more 17-AAG

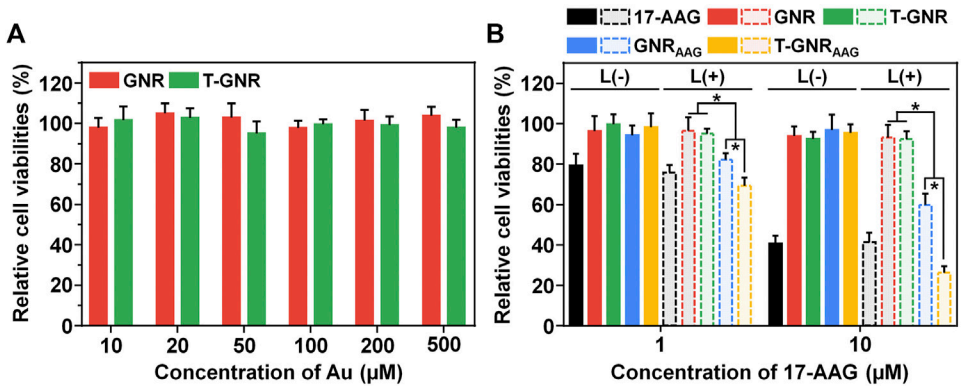

FIGURE 5 | (A) CCK-8 assay of GNR and T-GNR on HepG2 cells for 72 h. **(B)** Combined chemo-PTT effect of free 17-AAG, GNR, T-GNR, GNR_{AAG}, or $T\text{-}GNR_{AAG}$ against HepG2 cells upon 808 nm laser irradiation. *$p < 0.05$.

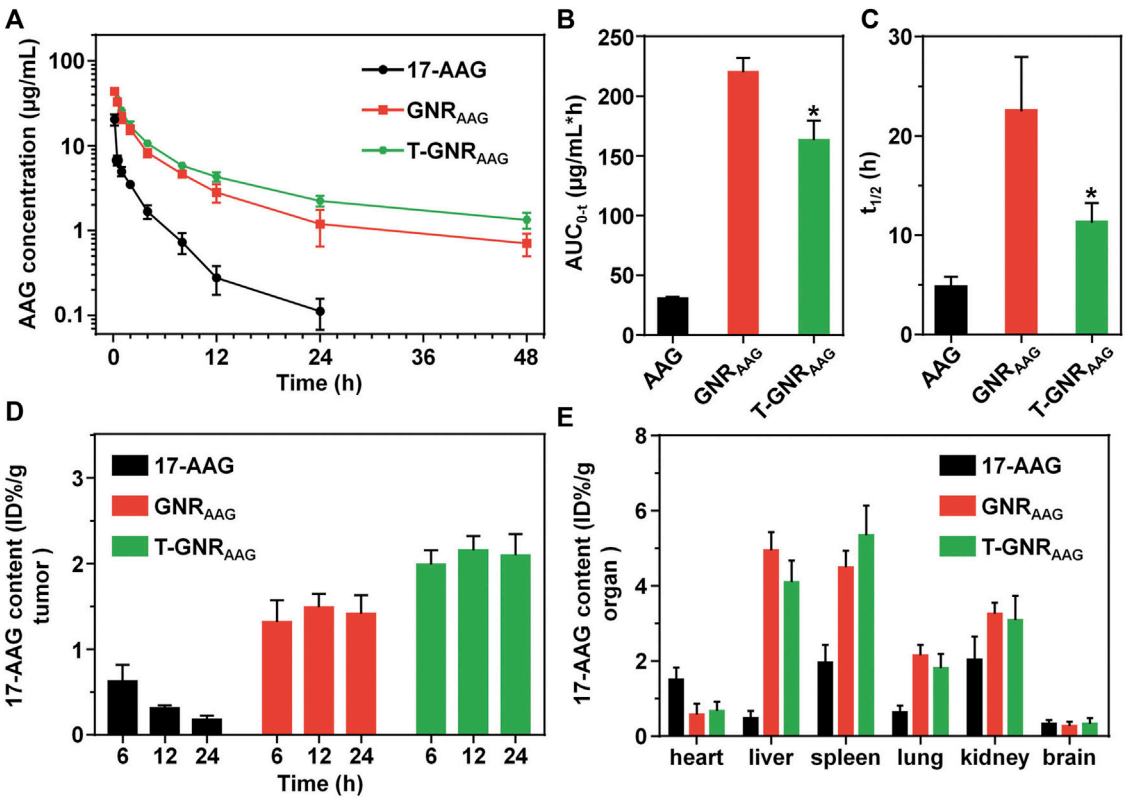

FIGURE 6 | (A) Plasma 17-AAG concentration vs. time after systemic administration of free 17-AAG, GNR_{AAG}, or $T\text{-}GNR_{AAG}$ (n = 4). The area under curve **(B)** and half-life **(C)** of free 17-AAG, GNR_{AAG}, and $T\text{-}GNR_{AAG}$. *$p < 0.05$ vs. GNR_{AAG}. **(D)** Quantitative 17-AAG content in HepG2 tumors at 6, 12, and 24 h postinjection. **(E)** Quantitative 17-AAG content in major organs of tumor-bearing mice at 24 h postinjection.

content in the $T\text{-}GNR_{AAG}$ group. In the presence of free LA, the internalization of $T\text{-}GNR_{AAG}$ was decreased to a level that was comparable to that of GNR_{AAG}, further suggesting the receptor-mediated endocytosis pathway of LA-decorated nanoparticles by HepG2 cells. Because of the absence of asialoglycoprotein receptor, the cellular uptake of GNR_{AAG} and $T\text{-}GNR_{AAG}$ was similar on Hela cells regardless of the presence of free LA (human cervical cancer cell line, **Supplementary Figure S3**). The advanced cellular uptake of T-GNR was further visualized using a CLSM. Because the fluorescence of 17-AAG is weak, ICG was used to replace 17-AAG for labeling the GNRs. As expected, there was a much greater ICG (red fluorescence)

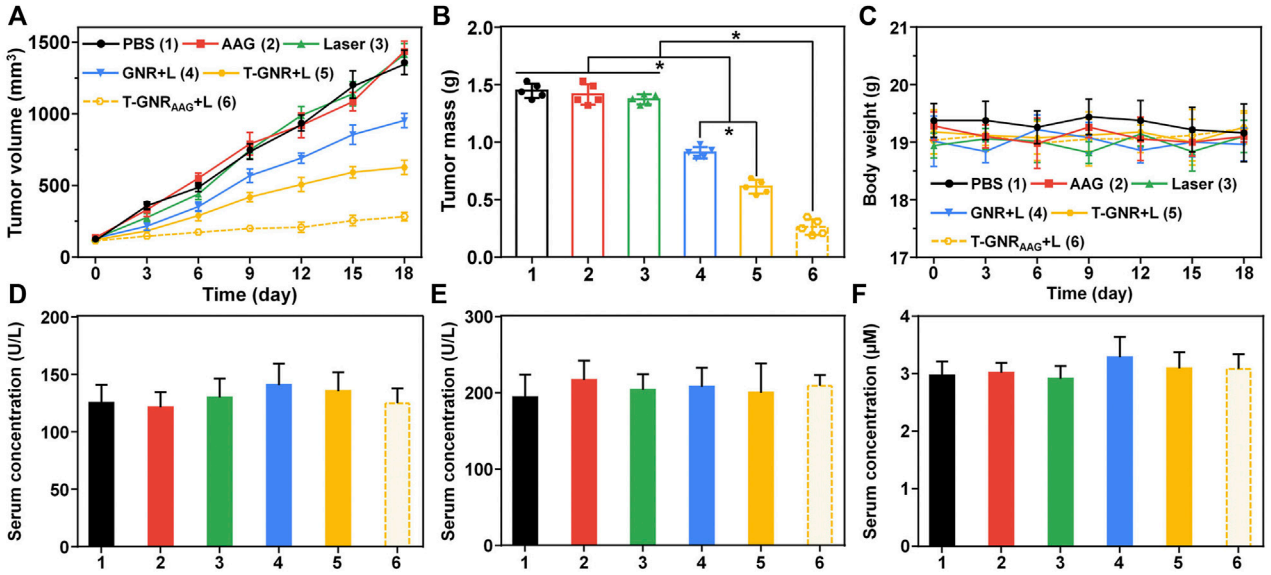

FIGURE 7 | (A) Tumor growth in HepG2 tumor xenograft-bearing BALB/c nude mice received various formulations. The *i.v.* injections were performed on day 0 (n = 5). **(B)** The HepG2 tumor mass after the treatment (day 18). *$p < 0.05$. **(C)** Body weight change of the mice during the therapeutic window. ELISA examination of ALT **(D)**, AST **(E),** and BUN **(F)** in the serum on day 18.

distribution localized inside the cytoplasm in the T-GNR_{ICG} group (**Figure 4C**).

Cell Killing Effect of T-GNR_{AAG} Under Laser Irradiation

According to our design, T-GNR_{AAG} would boost the antitumor activity *via* LA-promoted tumoral cell internalization. Then, the thermal effect generated from GNR under 808 nm laser irradiation liberated 17-AAG release and turned on subsequent Hsp90 inhibition and PTT-specific chemotherapy. The cytotoxicity of GNR and T-GNR without 17-AAG encapsulation was first measured on HepG2 cells through the CCK-8 assay. As shown in **Figure 5A**, insignificant cell viability change was observed even though the GNR concentration was 500 μM. Next, the HepG2 cells were incubated with free 17-AAG, GNR, T-GNR, GNR_{AAG}, or T-GNR_{AAG} and received 808 nm laser treatment (0.2 W/cm^2) for 10 min. Because the client proteins of Hsp90 were highly associated with tumoral cell proliferation (Talaei et al., 2019), free 17-AAG showed substantial cell killing regardless of laser irradiation (**Supplementary Figure S4**). The IC_{50} value of free 17-AAG was 7.63 μg/ml (L-). Upon laser irradiation, the negligible cell death of both the GNR + L and T-GNR + L groups suggested that such mild photothermal effect by a lower power density (0.2 W/cm^2) would not induce substantial damage against HepG2 cells (Zhong et al., 2013). More importantly, the significant difference between the GNR_{AAG} + L and T-GNR_{AAG} + L groups at both concentrations could be explained by the increased cellular uptake of T-GNR_{AAG} (**Figure 5B**). Compared to the T-GNR + L group, wherein chemotherapy was absent, the T-GNR_{AAG} + L group further exhibited more remarkable cell killing, with only 31.72 ± 4.45% of cell viability ([17-AAG] = 10.0 μM). To demonstrate the Hsp90 inhibition effect of 17-AAG, we analyzed the Hsp90 and its client protein (e.g., survivin and Akt) expression after the various treatments ([17-AAG] = 10 μM). As shown in **Supplementary Figure S5**, the expression of Hsp90, surviving, and Akt was elevated after PTT to enhance the thermal resistance but significantly decreased following incubation with free or released 17-AAG, which is in agreement with previous reports (Li et al., 2019; Sun et al., 2022). These results were consistent with both laser-activated drug release and cellular uptake experiments, verifying that the definitive cell killing efficacy of T-GNR_{AAG} + L is a result of both LA-facilitated agent delivery and combination chemo-PTT effect.

Pharmacokinetic and Biodistribution of T-GNR_{AAG} *In Vivo*

As expected, the nanocarriers with PEGylation would prolong the retention of chemotherapeutic agents in the bloodstream *via* reduced interaction with phagocytes. After systemic injection of different formulations, we collected the blood sample and measured the 17-AAG concentration in plasma at 0.17, 0.5, 1, 2, 4, 8, 12, 24, and 48 h. Because of the lower molecular weight, free 17-AAG was rapidly cleared from blood circulation even in the first 2 h (**Figure 6A**). The content of free 17-AAG was too low to be detected by UV-vis spectrophotometry at 48 h postinjection. On the other hand, both nanoparticular GNR_{AAG} and T-GNR_{AAG} maintained the 17-AAG concentration at 1.33 ± 0.28 and 0.70 ± 0.21 μg/ml at 48 h postinjection, respectively. Their difference after the 6 h time point could be attributed to the specific recognition and clearance of LA moiety. As shown in **Figure 6B**, we calculated their area under the curve (AUC_{0-t}) based on a noncompartmental model, and GNR_{AAG} and

T-GNR$_{AAG}$ were found to increase 7.21- and 5.35-folds of AUC_{0-t} than that of free 17-AAG (30.48 ± 1.34 μg/ml*h). Moreover, the $t_{1/2}$ of GNR$_{AAG}$ and T-GNR$_{AAG}$ was prolonged to 22.45 ± 5.50 and 11.23 ± 1.99 h, respectively (**Figure 6C**).

Taking advantage of the LA targeting ligand, T-GNR$_{AAG}$ has more opportunities to interact and be internalized by hepatoma cells. To demonstrate its tumor enriching, HepG2 tumor-bearing BALB/c nude mice were treated with GNR$_{AAG}$ or T-GNR$_{AAG}$ through *i.v.* injection, and the GNR content in major tissues and tumors was quantitatively determined by ICP-MS at 6, 12, and 24 h postinjection. As shown in **Figure 6D**, the 17-AAG content of GNR$_{AAG}$ was 1.31 ± 0.25, 1.49 ± 0.16, and 1.41 ± 0.22 %ID/g at 6, 12, and 24 h postinjection, respectively. However, the T-GNR$_{AAG}$ group exhibited a more pronounced tumor accumulation, whereas the 17-AAG concentration maintained to ca. 2.12 %ID/g tumor at both 12 and 24 h postinjection. As shown in **Figure 6E**, both GNR$_{AAG}$ and T-GNR$_{AAG}$ are preferentially distributed in reticuloendothelial system organs (i.e., spleen and liver), which is in line with previous reports (Ernsting et al., 2013; Li X. et al., 2020).

Tumor Growth Inhibition of T-GNR$_{AAG}$

Inspired by the superior effect of T-GNR$_{AAG}$ in blood circulation and biodistribution, we conducted antitumor experiments of T-GNR$_{AAG}$ *in vivo* using HepG2 tumor-bearing mice. Mice were randomly divided into six groups with five in each group. For both the GNR$_{AAG}$ + L and T-GNR$_{AAG}$ + L groups, mice received three dose of nano-formulation via intravenous administration on day 0, followed by the 808 nm laser irradiation (0.2 W/cm^2) for 10 min. During the laser irradiation, the mice that received an injection of T-GNR or T-GNR$_{AAG}$ exhibited the highest tumor temperature at ~42°C (**Supplementary Figure S6**). However, a limited PT effect was observed in mice injected with nontargeting GNR$_{AAG}$. As shown in **Figures 7A and B**, the tumor volume of mice treated with negative control groups grew rapidly, and the average tumor volume reached to ~1,350 mm^3 after 18 days. Owing to the moderate tumor accumulation, the GNR + L group showed partially tumor growth inhibition with a tumor inhibition rate (TIR) of 20.27%. With the help of LA-facilitated tumor enriching, the tumor volume in the T-GNR + L group was further decreased to about 950 mm^3 on day 18 after the single laser irradiation ($p > 0.05$ vs. the GNR + L group). More importantly, the T-GNR$_{AAG}$ + L group exhibited the most substantial tumor growth inhibition with a TIR of 70.45%. The comparison between the T-GNR + L and T-GNR$_{AAG}$ + L groups suggested that the antitumor effect was induced by a combination of PTT and chemotherapy, indicating the distinctly advanced therapeutic efficacy of such treatment. Furthermore, there was no substantial body weight loss for mice in all the groups on day 18 (**Figure 7C**). Additionally, liver/kidney function (**Figures 7D–F**) and blood routine count evaluation (**Supplementary Table S1**) verified the biocompatibility and biosafety of T-GNR$_{AAG}$ + L *in vivo*.

CONCLUSION

A targeted GNR has been developed for precise agent delivery and light-controlled drug release for combined chemo-PTT. After the LA modification, T-GNR$_{AAG}$ achieved more tumor enrichment *via* the LA-mediated targeting mechanism. Under 808 nm laser irradiation, T-GNR$_{AAG}$ not only achieved mild PTT for hepatocellular carcinoma but also accelerated the 17-AAG release for Hsp90 inhibition and PTT-specific chemotherapy *via* thermal-activated PCL phase transition. Considering the spatial directivity of the NIR laser, the combined chemo-PTT functioned within tumor regions, resulting in the advanced antitumor activity *in vivo*. Our work offers an attractive strategy for rational designing the remotely controlled nanocarriers for precise cancer therapy.

DATA AVAILABILITY STATEMENT

The raw data supporting the conclusions of this article will be made available by the authors, without undue reservation.

ETHICS STATEMENT

The animal study was reviewed and approved by the Tianjin Medical University Animal Care and Use Committee.

AUTHOR CONTRIBUTIONS

ZZ: conceptualization, investigation, writing–original draft, and writing–review and editing; CS: conceptualization, investigation, funding acquisition, supervision, and writing–review and editing.

FUNDING

This research was funded by the National Natural Science Foundation of China (82071907), Natural Science Foundation of Tianjin (18JCYBJC25100, 18JCQNJC80200), Health Science and Technology project of Tianjin (MS20022), Wu Jieping Medical Foundation Special Fund for Clinical Research (320.6750.2022-3-5), Tianjin Medical University General Hospital (ZYYFY2016041), and Tianjin Key Medical Discipline (Specialty) Construction Project.

SUPPLEMENTARY MATERIAL

The Supplementary Material for this article can be found online at: https://www.frontiersin.org/articles/10.3389/fmats.2022.931682/full#supplementary-material

REFERENCES

Abadeer, N. S., and Murphy, C. J. (2016). Recent Progress in Cancer Thermal Therapy Using Gold Nanoparticles. *J. Phys. Chem. C* 120, 4691–4716. doi:10.1021/acs.jpcc.5b11232

Almada, M., Leal-Martínez, B. H., Hassan, N., Kogan, M. J., Burboa, M. G., Topete, A., et al. (2017). Photothermal Conversion Efficiency and Cytotoxic Effect of Gold Nanorods Stabilized with Chitosan, Alginate and Poly(Vinyl Alcohol). *Mater. Sci. Eng. C* 77, 583–593. doi:10.1016/j.msec.2017.03.218

Chen, B.-Q., Kankala, R. K., Zhang, Y., Xiang, S.-T., Tang, H.-X., Wang, Q., et al. (2020). Gambogic Acid Augments Black Phosphorus Quantum Dots (BPQDs)-Based Synergistic Chemo-Photothermal Therapy through Downregulating Heat Shock Protein Expression. *Chem. Eng. J.* 390, 124312. doi:10.1016/j.cej.2020.124312

Chen, Q., Xu, L., Liang, C., Wang, C., Peng, R., and Liu, Z. (2016). Photothermal Therapy with Immune-Adjuvant Nanoparticles Together with Checkpoint Blockade for Effective Cancer Immunotherapy. *Nat. Commun.* 7, 13193. doi:10.1038/ncomms13193

Dong, S., Dong, Y., Jia, T., Liu, S., Liu, J., Yang, D., et al. (2020). GSH-Depleted Nanozymes with Hyperthermia-Enhanced Dual Enzyme-Mimic Activities for Tumor Nanocatalytic Therapy. *Adv. Mat.* 32, 2002439. doi:10.1002/adma.202002439

Doughty, A., Hoover, A., Layton, E., Murray, C., Howard, E., and Chen, W. (2019). Nanomaterial Applications in Photothermal Therapy for Cancer. *Materials* 12, 779. doi:10.3390/ma12050779

Ernsting, M. J., Murakami, M., Roy, A., and Li, S.-D. (2013). Factors Controlling the Pharmacokinetics, Biodistribution and Intratumoral Penetration of Nanoparticles. *J. Control. Release* 172, 782–794. doi:10.1016/j.jconrel.2013.09.013

Ferrario, A., and Gomer, C. J. (2010). Targeting the 90kDa Heat Shock Protein Improves Photodynamic Therapy. *Cancer Lett.* 289, 188–194. doi:10.1016/j.canlet.2009.08.015

Gao, G., Jiang, Y. W., Sun, W., Guo, Y., Jia, H. R., Yu, X. W., et al. (2019). Molecular Targeting-Mediated Mild-Temperature Photothermal Therapy with a Smart Albumin-Based Nanodrug. *Small* 15, 1900501. doi:10.1002/smll.201900501

Georgakis, G. V., Li, Y., Rassidakis, G. Z., Martinez-Valdez, H., Medeiros, L. J., and Younes, A. (2006). Inhibition of Heat Shock Protein 90 Function by 17-Allylamino-17-Demethoxy-Geldanamycin in Hodgkin's Lymphoma Cells Down-Regulates Akt Kinase, Dephosphorylates Extracellular Signal-Regulated Kinase, and Induces Cell Cycle Arrest and Cell Death. *Clin. Cancer Res.* 12, 584–590. doi:10.1158/1078-0432.CCR-05-1194

Hasenstein, J. R., Shin, H.-C., Kasmerchak, K., Buehler, D., Kwon, G. S., and Kozak, K. R. (2012). Antitumor Activity of Triolimus: A Novel Multidrug-Loaded Micelle Containing Paclitaxel, Rapamycin, and 17-AAG. *Mol. Cancer Ther.* 11, 2233–2242. doi:10.1158/1535-7163.MCT-11-0987

He, C., Sun, J., Deng, C., Zhao, T., Deng, M., Chen, X., et al. (2004). Study of the Synthesis, Crystallization, and Morphology of Poly(ethylene glycol)−Poly(ε-Caprolactone) Diblock Copolymers. *Biomacromolecules* 5, 2042–2047. doi:10.1021/bm049720e

He, J., Qiao, Y., Zhang, H., Zhao, J., Li, W., Xie, T., et al. (2020a). Gold-silver Nanoshells Promote Wound Healing from Drug-Resistant Bacteria Infection and Enable Monitoring via Surface-Enhanced Raman Scattering Imaging. *Biomaterials* 234, 119763. doi:10.1016/j.biomaterials.2020.119763

He, J., Shi, M., Liang, Y., and Guo, B. (2020b). Conductive Adhesive Self-Healing Nanocomposite Hydrogel Wound Dressing for Photothermal Therapy of Infected Full-Thickness Skin Wounds. *Chem. Eng. J.* 394, 124888. doi:10.1016/j.cej.2020.124888

Huang, S., Ma, P. a., Wei, Y., Cheng, Z., Liu, B., Deng, X., et al. (2020). Controllable Synthesis of Hollow Porous Silica Nanotubes/CuS Nanoplatform for Targeted Chemo-Photothermal Therapy. *Sci. China Mat.* 63, 864–875. doi:10.1007/s40843-019-1235-1

Jang, B., Park, J.-Y., Tung, C.-H., Kim, I.-H., and Choi, Y. (2011). Gold Nanorod–Photosensitizer Complex for Near-Infrared Fluorescence Imaging and Photodynamic/Photothermal Therapy *In Vivo*. *ACS Nano* 5, 1086–1094. doi:10.1021/nn102722z

Kamal, A., Thao, L., Sensintaffar, J., Zhang, L., Boehm, M. F., Fritz, L. C., et al. (2003). A High-Affinity Conformation of Hsp90 Confers Tumour Selectivity on Hsp90 Inhibitors. *Nature* 425, 407–410. doi:10.1038/nature01913

Lamb, J., Crawford, E. D., Peck, D., Modell, J. W., Blat, I. C., Wrobel, M. J., et al. (2006). The Connectivity Map: Using Gene-Expression Signatures to Connect Small Molecules, Genes, and Disease. *Science* 313, 1929–1935. doi:10.1126/science.1132939

Li, J., and Kataoka, K. (2021). Chemo-physical Strategies to Advance the *In Vivo* Functionality of Targeted Nanomedicine: The Next Generation. *J. Am. Chem. Soc.* 143, 538–559. doi:10.1021/jacs.0c09029

Li, J., and Pu, K. (2020). Semiconducting Polymer Nanomaterials as Near-Infrared Photoactivatable Protherapeutics for Cancer. *Acc. Chem. Res.* 53, 752–762. doi:10.1021/acs.accounts.9b00569

Li, L., Wang, L., You, Q.-D., and Xu, X.-L. (2020). Heat Shock Protein 90 Inhibitors: An Update on Achievements, Challenges, and Future Directions. *J. Med. Chem.* 63, 1798–1822. doi:10.1021/acs.jmedchem.9b00940

Li, W.-q., Sun, C.-y., Wang, F., Wang, Y.-c., Zhai, Y.-w., Liang, M., et al. (2013). Achieving a New Controllable Male Contraception by the Photothermal Effect of Gold Nanorods. *Nano Lett.* 13, 2477–2484. doi:10.1021/nl400536d

Li, X., Wang, B., Zhou, S., Chen, W., Chen, H., Liang, S., et al. (2020). Surface Chemistry Governs the Sub-organ Transfer, Clearance and Toxicity of Functional Gold Nanoparticles in the Liver and Kidney. *J. Nanobiotechnol* 18, 45. doi:10.1186/s12951-020-00599-1

Li, Z., Jia, L., Tang, H., Shen, Y., and Shen, C. (2019). Synthesis and Biological Evaluation of Geldanamycin-Ferulic Acid Conjugate as a Potent Hsp90 Inhibitor. *RSC Adv.* 9, 42509–42515. doi:10.1039/C9RA08665J

Lin, T.-y., Guo, W., Long, Q., Ma, A., Liu, Q., Zhang, H., et al. (2016). HSP90 Inhibitor Encapsulated Photo-Theranostic Nanoparticles for Synergistic Combination Cancer Therapy. *Theranostics* 6, 1324–1335. doi:10.7150/thno.14882

Liu, H., Wang, H., Xu, Y., Guo, R., Wen, S., Huang, Y., et al. (2014). Lactobionic Acid-Modified Dendrimer-Entrapped Gold Nanoparticles for Targeted Computed Tomography Imaging of Human Hepatocellular Carcinoma. *ACS Appl. Mat. Interfaces* 6, 6944–6953. doi:10.1021/am500761x

Liu, J., Detrembleur, C., Grignard, B., De Pauw-Gillet, M.-C., Mornet, S., Treguer-Delapierre, M., et al. (2014). Gold Nanorods with Phase-Changing Polymer Corona for Remotely Near-Infrared-Triggered Drug Release. *Chem. Asian J.* 9, 275–288. doi:10.1002/asia.201301010

Liu, S., Zhou, X., Zhang, H., Ou, H., Lam, J. W. Y., Liu, Y., et al. (2019). Molecular Motion in Aggregates: Manipulating TICT for Boosting Photothermal Theranostics. *J. Am. Chem. Soc.* 141, 5359–5368. doi:10.1021/jacs.8b13889

Liu, Y., Suo, X., Peng, H., Yan, W., Li, H., Yang, X., et al. (2019). Multifunctional Magnetic Nanoplatform Eliminates Cancer Stem Cells via Inhibiting the Secretion of Extracellular Heat Shock Protein 90. *Adv. Healthc. Mat.* 8, 1900160. doi:10.1002/adhm.201900160

Long, Q., Lin, T.-y., Huang, Y., Li, X., Ma, A.-h., Zhang, H., et al. (2018). Image-Guided Photo-Therapeutic Nanoporphyrin Synergized HSP90 Inhibitor in Patient-Derived Xenograft Bladder Cancer Model. *Nanomedicine Nanotechnol. Biol. Med.* 14, 789–799. doi:10.1016/j.nano.2017.12.014

Modi, S., Stopeck, A., Linden, H., Solit, D., Chandarlapaty, S., Rosen, N., et al. (2011). HSP90 Inhibition Is Effective in Breast Cancer: A Phase II Trial of Tanespimycin (17-AAG) Plus Trastuzumab in Patients with HER2-Positive Metastatic Breast Cancer Progressing on Trastuzumab. *Clin. Cancer Res.* 17, 5132–5139. doi:10.1158/1078-0432.CCR-11-0072

Rochani, A. K., Balasubramanian, S., Ravindran Girija, A., Raveendran, S., Borah, A., Nagaoka, Y., et al. (2016). Dual Mode of Cancer Cell Destruction for Pancreatic Cancer Therapy Using Hsp90 Inhibitor Loaded Polymeric Nano Magnetic Formulation. *Int. J. Pharm.* 511, 648–658. doi:10.1016/j.ijpharm.2016.07.048

Saxena, V., Naguib, Y., and Hussain, M. D. (2012). Folate Receptor Targeted 17-Allylamino-17-Demethoxygeldanamycin (17-AAG) Loaded Polymeric Nanoparticles for Breast Cancer. *Colloids Surfaces B Biointerfaces* 94, 274–280. doi:10.1016/j.colsurfb.2012.02.001

Shan, X., Zhang, X., Wang, C., Zhao, Z., Zhang, S., Wang, Y., et al. (2021). Molecularly Engineered Carrier-free Co-delivery Nanoassembly for Self-Sensitized Photothermal Cancer Therapy. *J. Nanobiotechnol* 19, 282. doi:10.1186/s12951-021-01037-6

Sun, H., Zhang, Q., Li, J., Peng, S., Wang, X., and Cai, R. (2021). Near-Infrared Photoactivated Nanomedicines for Photothermal Synergistic Cancer Therapy. *Nano Today* 37, 101073. doi:10.1016/j.nantod.2020.101073

Sun, Q., Liu, F., Wen, Z., Xia, J., Li, H., Xu, Y., et al. (2022). Combined Effect of Heat Shock Protein Inhibitor Geldanamycin and Free Radicals on Photodynamic Therapy of Prostate Cancer. *J. Mat. Chem. B* 10, 1369–1377. doi:10.1039/d1tb02219a

Sun, T., Chen, X., Wang, X., Liu, S., Liu, J., and Xie, Z. (2019). Enhanced Efficacy of Photothermal Therapy by Combining a Semiconducting Polymer with an Inhibitor of a Heat Shock Protein. *Mat. Chem. Front.* 3, 127–136. doi:10.1039/c8qm00459e

Talaei, S., Mellatyar, H., Asadi, A., Akbarzadeh, A., Sheervalilou, R., and Zarghami, N. (2019). Spotlight on 17-AAGas an Hsp90 Inhibitor for Molecular Targeted Cancer Treatment. *Chem. Biol. Drug Des.* 93, 760–786. doi:10.1111/cbdd.13486

Wang, H., Chang, J., Shi, M., Pan, W., Li, N., and Tang, B. (2019). A Dual-Targeted Organic Photothermal Agent for Enhanced Photothermal Therapy. *Angew. Chem. Int. Ed.* 58, 1057–1061. doi:10.1002/anie.201811273

Waza, M., Adachi, H., Katsuno, M., Minamiyama, M., Sang, C., Tanaka, F., et al. (2005). 17-AAG, an Hsp90 Inhibitor, Ameliorates Polyglutamine-Mediated Motor Neuron Degeneration. *Nat. Med.* 11, 1088–1095. doi:10.1038/nm1298

Whitesell, L., and Lindquist, S. L. (2005). HSP90 and the Chaperoning of Cancer. *Nat. Rev. Cancer* 5, 761–772. doi:10.1038/nrc1716

Xi, D., Xiao, M., Cao, J., Zhao, L., Xu, N., Long, S., et al. (2020). NIR Light-Driving Barrier-free Group Rotation in Nanoparticles with an 88.3% Photothermal Conversion Efficiency for Photothermal Therapy. *Adv. Mater* 32, e1907855. doi:10.1002/adma.201907855

Xie, Z., Fan, T., An, J., Choi, W., Duo, Y., Ge, Y., et al. (2020). Emerging Combination Strategies with Phototherapy in Cancer Nanomedicine. *Chem. Soc. Rev.* 49, 8065–8087. doi:10.1039/d0cs00215a

Yang, J.-C., Chen, Y., Li, Y.-H., and Yin, X.-B. (2017). Magnetic Resonance Imaging-Guided Multi-Drug Chemotherapy and Photothermal Synergistic Therapy with pH and NIR-Stimulation Release. *ACS Appl. Mat. Interfaces* 9, 22278–22288. doi:10.1021/acsami.7b06105

Yang, Y., Xu, M., Wang, Z., Yang, Y., Liu, J., Hu, Q., et al. (2021). Immune Remodeling Triggered by Photothermal Therapy with Semiconducting Polymer Nanoparticles in Combination with Chemotherapy to Inhibit Metastatic Cancers. *J. Mat. Chem. B* 9, 2613–2622. doi:10.1039/d0tb02903c

Yang, Y., Zhu, W., Dong, Z., Chao, Y., Xu, L., Chen, M., et al. (2017). 1D Coordination Polymer Nanofibers for Low-Temperature Photothermal Therapy. *Adv. Mat.* 29, 1703588. doi:10.1002/adma.201703588

Yi, Y., Wang, H., Wang, X., Liu, Q., Ye, M., and Tan, W. (2017). A Smart, Photocontrollable Drug Release Nanosystem for Multifunctional Synergistic Cancer Therapy. *ACS Appl. Mat. Interfaces* 9, 5847–5854. doi:10.1021/acsami.6b15414

Zhang, H., Zhang, Q., Liu, C., and Han, B. (2019). Preparation of a One-Dimensional Nanorod/metal Organic Framework Janus Nanoplatform via Side-specific Growth for Synergistic Cancer Therapy. *Biomater. Sci.* 7, 1696–1704. doi:10.1039/c8bm01591k

Zhang, X., Tang, J., Li, C., Lu, Y., Cheng, L., and Liu, J. (2021). A Targeting Black Phosphorus Nanoparticle Based Immune Cells Nano-Regulator for Photodynamic/Photothermal and Photo-Immunotherapy. *Bioact. Mater.* 6, 472–489. doi:10.1016/j.bioactmat.2020.08.024

Zhong, Y., Wang, C., Cheng, L., Meng, F., Zhong, Z., and Liu, Z. (2013). Gold Nanorod-Cored Biodegradable Micelles as a Robust and Remotely Controllable Doxorubicin Release System for Potent Inhibition of Drug-Sensitive and -Resistant Cancer Cells. *Biomacromolecules* 14, 2411–2419. doi:10.1021/bm400530d

Zhu, X., Guan, B., Sun, Z., Tian, X., and Li, X. (2021). Fabrication of an Injectable Hydrogel with Inherent Photothermal Effects from Tannic Acid for Synergistic Photothermal-Chemotherapy. *J. Mat. Chem. B* 9, 6084–6091. doi:10.1039/D1TB01057C

Conflict of Interest: The authors declare that the research was conducted in the absence of any commercial or financial relationships that could be construed as a potential conflict of interest.

Publisher's Note: All claims expressed in this article are solely those of the authors and do not necessarily represent those of their affiliated organizations or those of the publisher, the editors, and the reviewers. Any product that may be evaluated in this article, or claim that may be made by its manufacturer, is not guaranteed or endorsed by the publisher.